Supplementary Information

Impacts of a weakened AMOC on precipitation over the Euro-Atlantic region in the EC-Earth3 climate model

Authors

Katinka Bellomo[1,2*], Virna L. Meccia[3], Roberta D'Agostino[4,5], Federico Fabiano[3], Sarah M. Larson[6], Jost von Hardenberg[1,2], Susanna Corti[3]

[1] Polytechnic University of Turin, Department of Environment, Land and Infrastructure Engineering, Turin, Italy
[2] National Research Council, Institute of Atmospheric Sciences and Climate, Turin, Italy
[3] National Research Council, Institute of Atmospheric Sciences and Climate, Bologna, Italy
[4] University of Trento, Department of Civil, Environmental and Mechanical Engineering, Trento, Italy
[5] Max-Planck Institute for Meteorology, Hamburg, Germany
[6] Department of Marine, Earth, and Atmospheric Sciences, North Carolina State University, Raleigh, NC, USA

*corresponding author: katinka.bellomo@polito.it

EC-Earth3 response to freshwater hosing

In fig. S1 we show that although the AMOC index exhibits a steady decline, EC-Earth3 reacts to the freshwater flux by temporarily shifting the deep convection in the North Atlantic towards higher latitudes, similar to other models (e.g., Stouffer et al. 2006). This leads to decades in which the mean air temperature increases, an effect that is amplified by sea-ice melting. Fig. S1a shows the timeseries of the near-surface air temperature averaged over the representative region 70°-80°N, 15°W-37°E (boxed in fig. S1b and S1d). The black curve in fig. S1a represents the timeseries of near-surface air temperature in the control simulation, while the grey curve represents the same variable but for the water hosing experiment. For reference, the horizontal line represents the mean value in the control simulation (-8.66 °C). Fig. S1a shows that in the first 30 years of the water hosing experiment the air temperature decreases over this region, as well as in the rest of the Northern Hemisphere. However, after year 30 air temperature starts rising, only to drop below the horizontal line again at year 95. Hence, for about 65 years, there is a positive near-surface air temperature anomaly in this region. We note that at year 140, air temperature in fig. S1a starts rising again because at that year the water hosing is halted, as explained in the main text.

Figs. S1b and S1d show composites of winter (DJFM) near-surface air temperature anomalies (shading) and sea-ice cover (contours) during warm (fig. S1b) and cold (fig. S1d) years of the water hosing experiment. Anomalies are computed with respect to the control mean climate. Warm years are selected as the years in which the air temperature plotted in fig. S1a (boxed region) is warmer than the long-term mean control temperature in this same region (i.e., above the horizontal line in fig. S1a). For the cold period we composite over the years 100-159, when the near-surface air temperature is below the climatology (fig. S1a), but also when the AMOC is weaker than 50% compared to the control climate. We choose to show this time period (years 100-159) to be consistent with panels shown in fig. 2 and the rest of the analysis; however, these and the following results in this section are similar if we instead consider all years in which the near-surface air temperature time series in fig. S1a is colder than the climatology (i.e., below the horizontal line in fig. S1a). The average seasonal mean (DJFM) air temperature change in the boxed region is +2.78 °C (fig. S1b) for the warm years composite, while it is -8.23 °C (fig. S1d) for the cold years composite. Instead, the average seasonal mean (DJFM) sea ice concentration change is -18.65% for the warm years (fig. S1b), and +31.62% for the cold years (fig. S1d). Hence, anomalies in sea ice concentration tend to amplify temperature anomalies.

We suspect that the increase in near-surface air temperature after year 30 is due to a temporary reactivation of the overturning ocean circulation at high latitudes. Fig. S1c shows the meridional ocean heat transport (OHT) in the Atlantic/Arctic sector and provides evidence for a transient northward shift in deep convection. This can be seen from the OHT anomaly in the warm years (dashed red curve in fig. S1c) compared to the cold years (dashed blue curve in fig. S1c). The dashed red anomalies (composite of warm years) in fig. S1c are positive between ~60°N and ~80°N, indicating enhanced northward OHT. On the contrary, the dashed blue anomalies (composite of cold years) in fig. S1c are negative at about the same latitudes, indicating reduced northward OHT. To corroborate this hypothesis, we show in fig. S2 composites of salinity and mixed-layer depth anomalies. The composites show increased salinity and deeper mixed layer depths in the Norwegian and Barents seas during the warm years, thus providing further evidence for a temporary recovery of deep convection at higher latitudes.

Additional hosing suppresses the temporary recovery of deep convection at higher latitudes, as can be seen from the composites of the cold years in fig. S1d and fig. S2, but when the hosing stops at year 140, the AMOC starts recovering to its original strength. The northward shift in deep convection is a response that is shared with other models (see Stouffer et al. 2006 and Jackson et al. 2022), but the mechanisms are yet to be clarified. A previous study by van der Berk et al. (2021) performed a more realistic water hosing model experiment with the coupled climate model EC-Earth2.2 in a future RCP8.5 emission scenario to simulate Greenland ice sheet mass loss. Their study shows a similar response to the water hosing forcing as in the present study, despite the different model version and background climate. They show that the AMOC is only slightly affected by the imposed forcing because of enhanced convection and stronger overflows in the Nordic Seas, which also lead to warmer subpolar SSTs. However, we leave an in-depth analysis of AMOC recovery mechanisms in EC-Earth3 for a future study. Here instead we analyze the impacts of a weakened AMOC, with a focus on precipitation (main text).

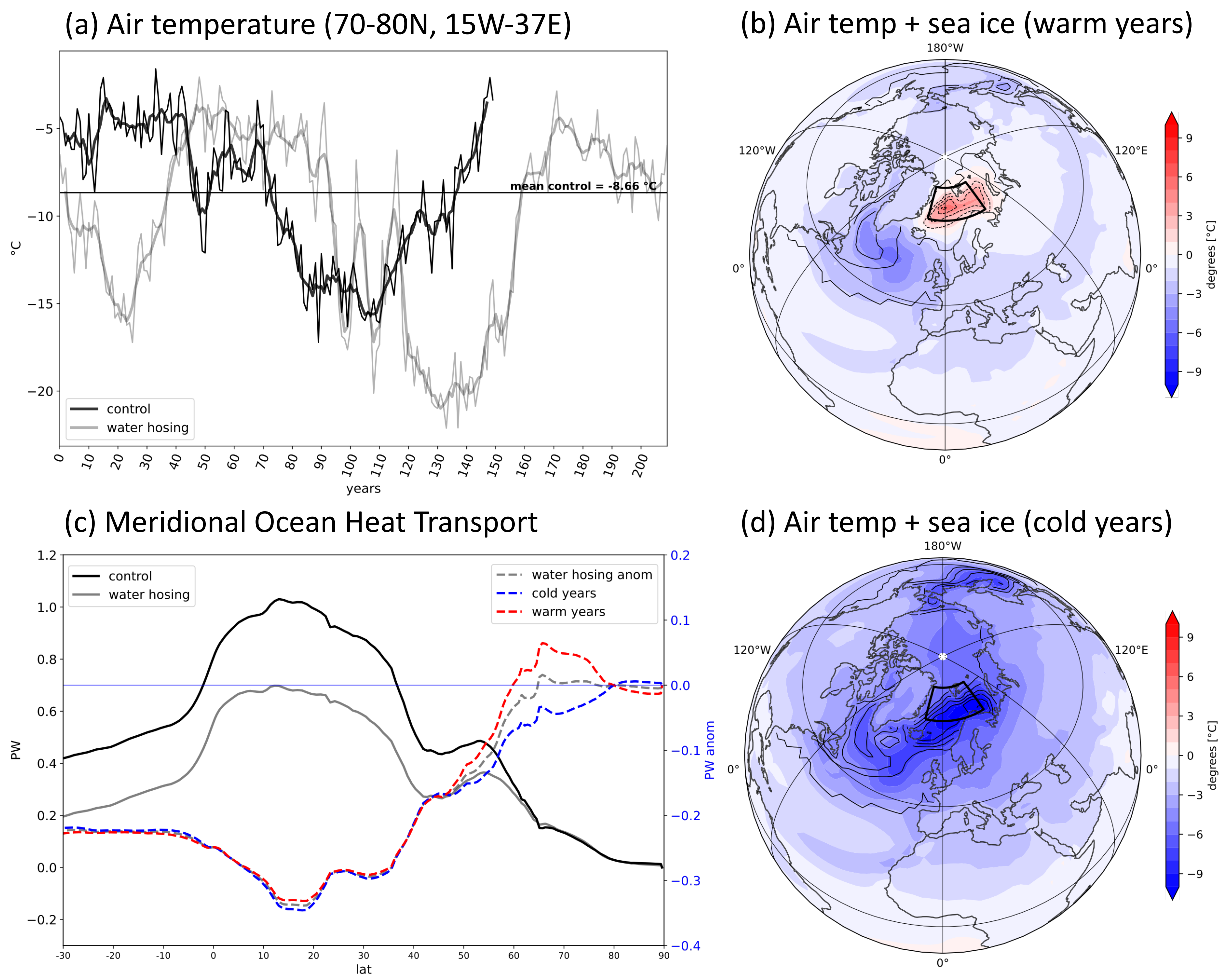

Fig. S1: Temporary overturning recovery. (a): Timeseries of near-surface air temperature in DJFM averaged over the boxed area in panel (b). Superimposed to annual mean values are 5 years running averages of the timeseries; (b) and (d): Composites of near-surface air temperature (shading) and sea-ice cover (contours) anomalies in DJFM during (b) warm years and (d) cold years of the water hosing experiment. Anomalies in the water hosing experiment are computed with respect to the control climatology. Sea-ice cover is in units of % and levels are plotted every 10% ; (c) Zonal mean average of the annual mean ocean meridional heat transport (OHT) in the Atlantic/Arctic sector. The black and gray curves refer to the left side y-axis and are absolute values of the OHT in the control and water hosing experiments, respectively. The dashed curves are anomalies in the water hosing experiment and refer to the right side y-axis.

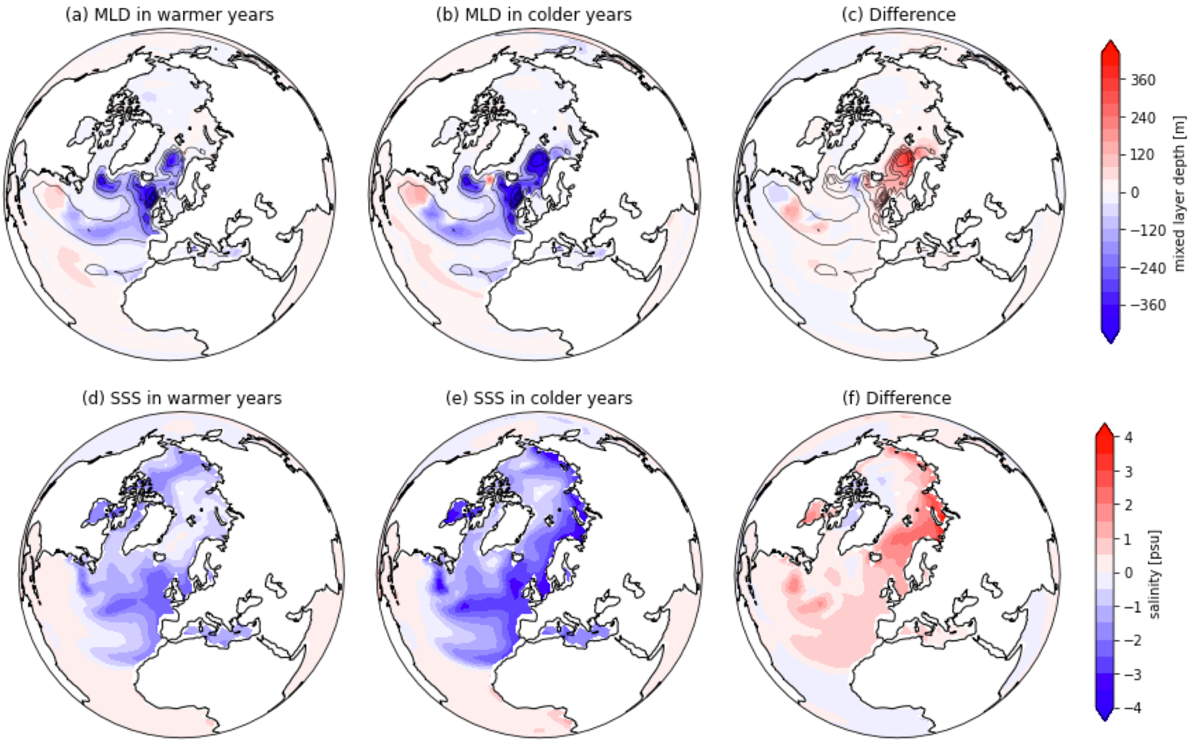

Fig. S2: Diagnostics of temporary AMOC recovery. Top row panels show the March mixed-layer depth composites in (a) warm years, (b) cold years, and (c) their difference. Solid contours represent the climatology computed from the control simulation; Bottom row panels show the DJFM sea-surface salinity composites in (d) warm years, (e) cold years, and (f) their difference. Composites are computed as explained in the introductory paragraph and in the caption of fig. S1. Anomalies are computed with respect to the control climatology.

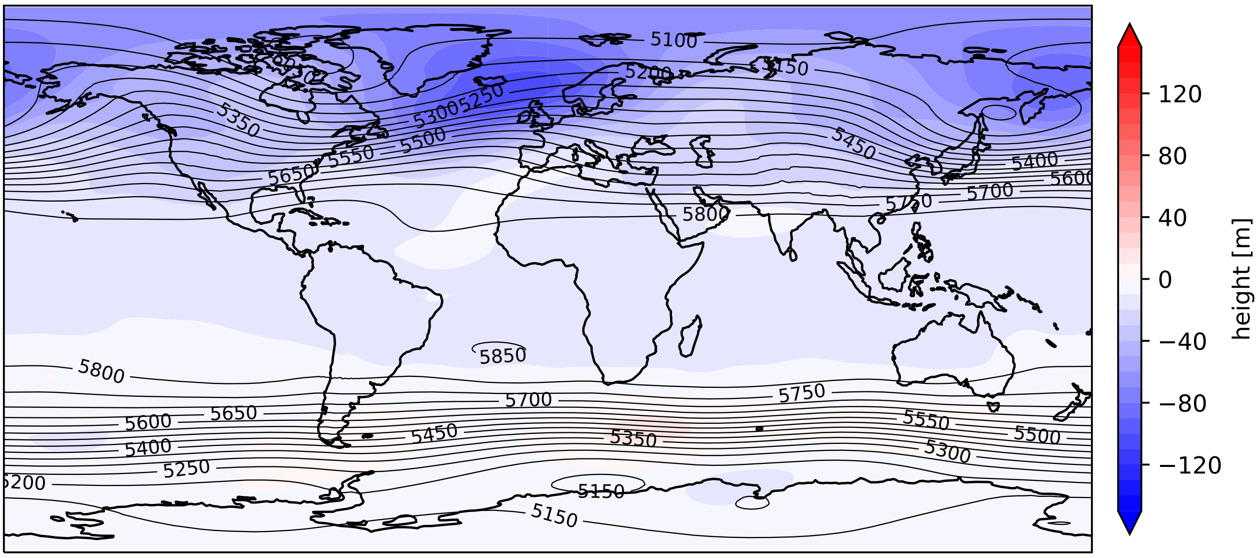

Fig. S3: Change in geopotential height (at 500m) in DJFM (water hosing minus control). Shaded colors indicate the change in geopotential height, while solid contours show the climatology computed from the control simulation.

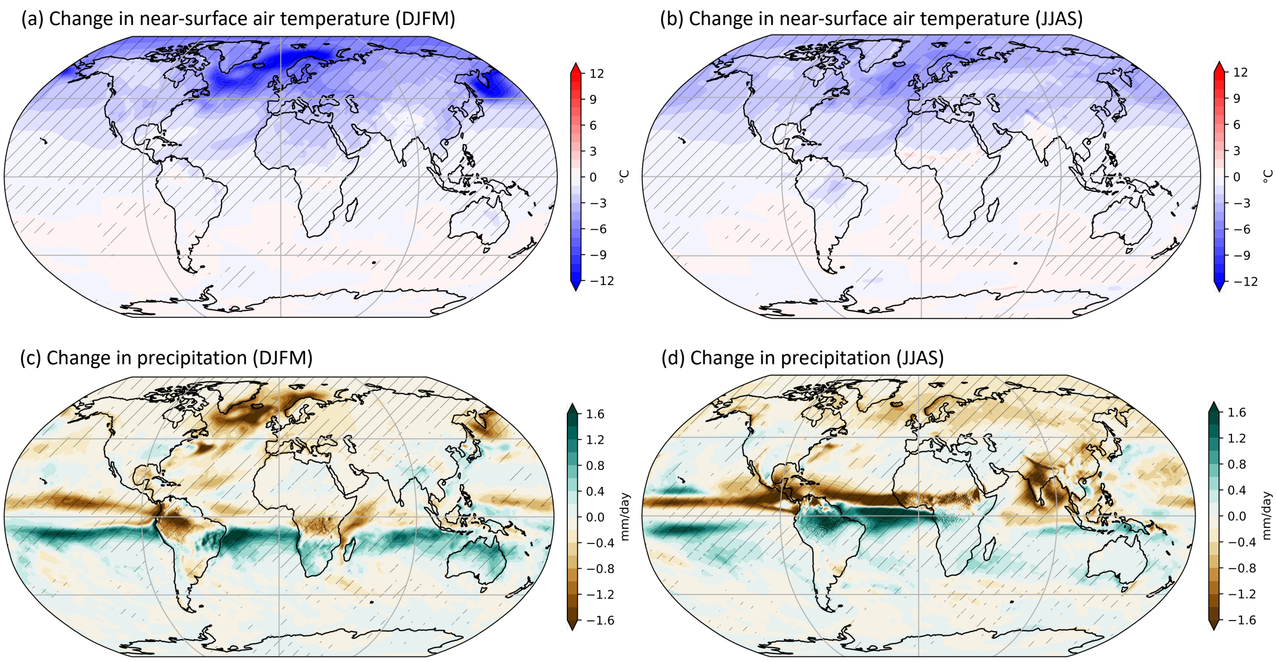

Fig. S4: Seasonal changes (water hosing minus control). (a) DJFM change in near-surface temperature; (b) same as in (a) but in JJAS; (c) DJFM change in precipitation; (d) same as (c) but for JJAS. Hashes indicate statistical significance. The change in near-surface temperature in DJFM is -1.25 °C for the global mean, -2.42 °C averaged over the Northern Hemisphere, -0.07 °C averaged over the Southern Hemisphere. The change in near-surface temperature in JJAS is -0.94 °C for the global mean, -1.74 °C averaged over the Northern Hemisphere, -0.13 °C averaged over the Southern Hemisphere.

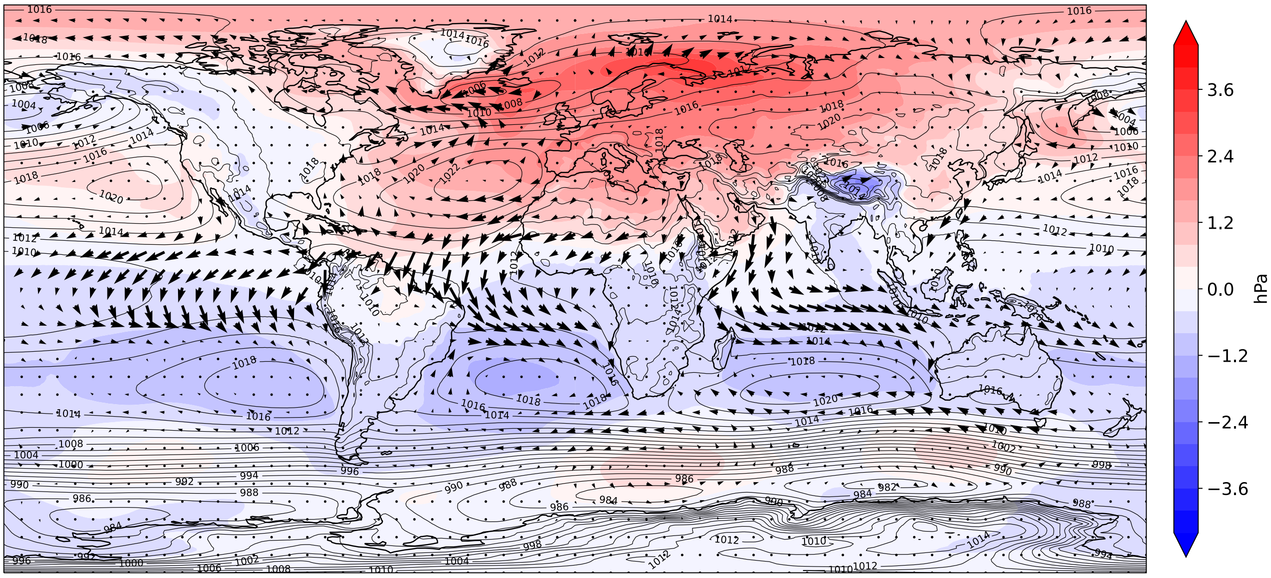

Fig. S5: Change in annual mean SLP (water hosing minus control). Shaded colors indicate changes in sea level pressure (SLP), while vectors indicate change in surface winds. Superimposed in contours is the annual mean SLP climatology.

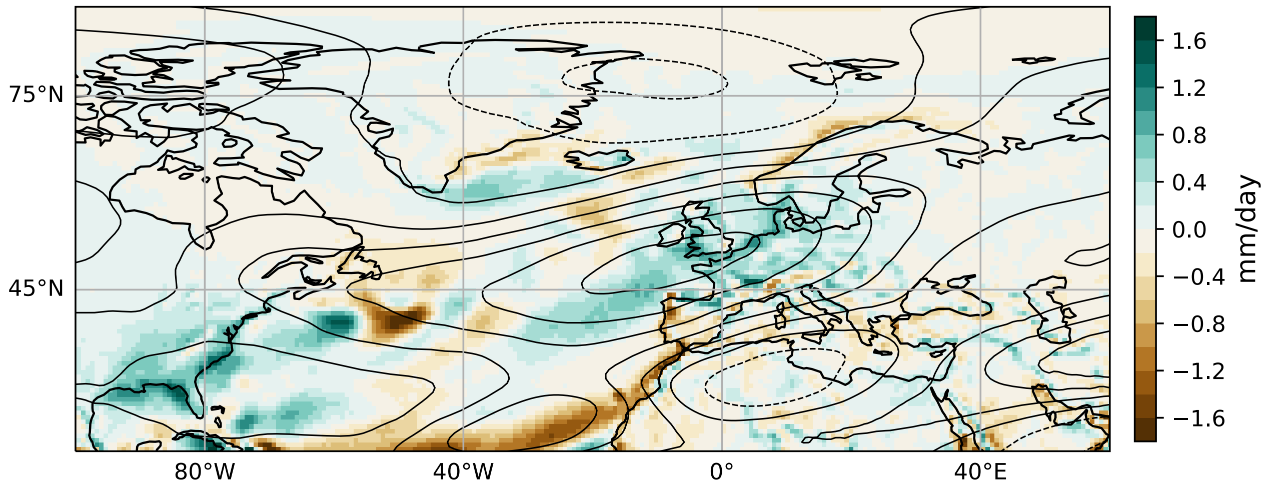

Fig. S6: Dynamic contributions (water hosing minus control). Shaded colors indicate changes in the dynamic term of the moisture budget (same as fig. 6b), while contours indicate change in the zonal wind at 250hPa (same as shading in fig. 9a). This figure shows the co-location of the enhanced jet stream and the dynamic term in northwestern Europe, both promoting a regional increase in net precipitation anomalies.

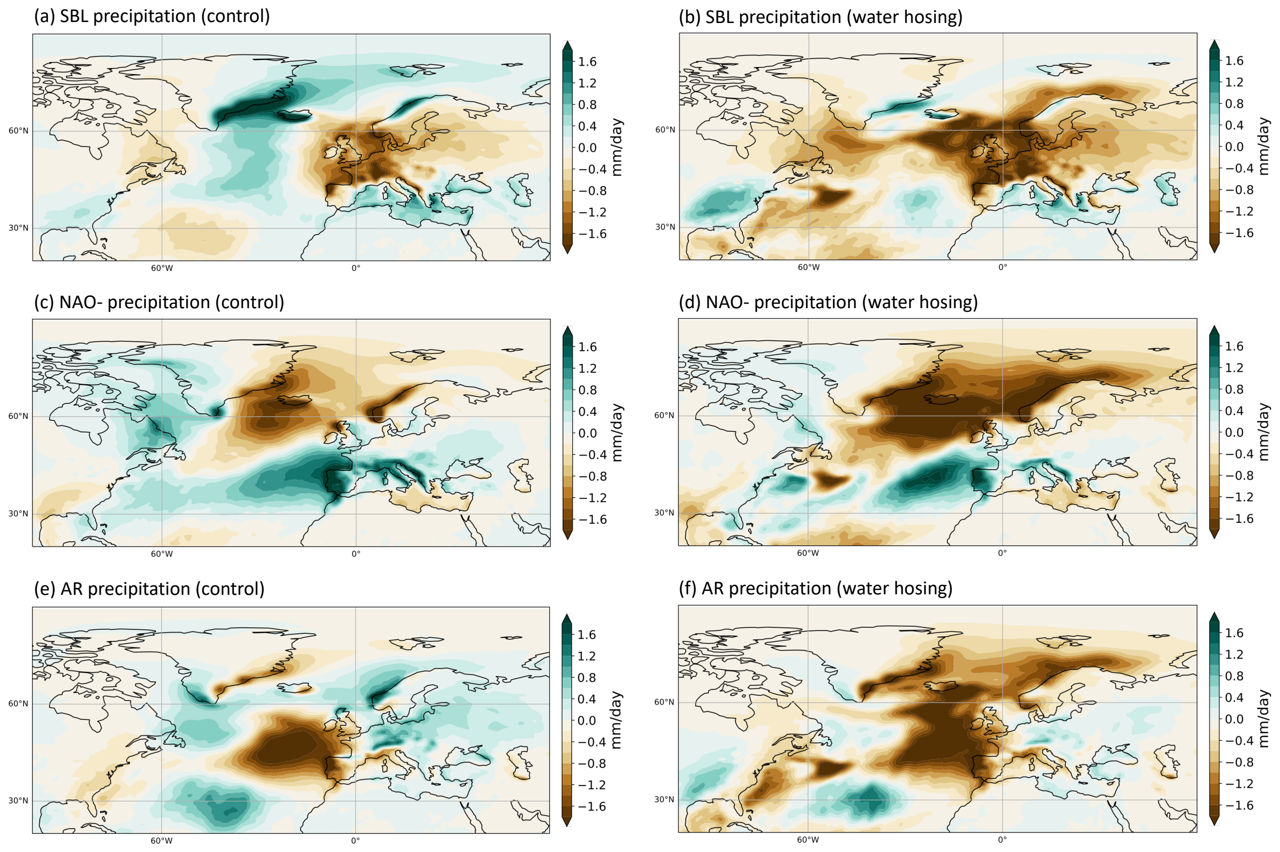

Fig. S7: Precipitation anomalies composites. All composites are obtained averaging daily anomalies computed against the control climatology over the days assigned to the each WR. (a) and (b): Scandinavian Blocking (SBL) in control and water hosing experiments, respectively; (c) and (d): same as top row but for the negative phase of the North Atlantic Oscillation (NAO-); (e) and (f): same as top row but for Atlantic Ridge (AR).

Table S1: Statistics related to the frequency of WRs in DJFM (fig. 11).

Frequency [%]	**NAO+**		**SBL**		**NAO-**		**AR**	
	Experiment		*Experiment*		*Experiment*		*Experiment*	
	control	hosing	control	hosing	control	hosing	control	hosing
Mean	26.7	42.8	25.1	18.0	24.8	16.6	23.5	22.5
Median	24.8	43.0	23.1	17.4	24.8	14.0	22.3	21.5
25^{th}-75^{th} percentile range	17.4-34.7	34.3-49.2	18.2-30.6	12.0-24.0	14.0-33.1	8.3-21.9	17.4-30.6	15.7-27.7
10^{th}-90^{th} percentile range	10.6-44.8	29.8-58.8	13.2-39.7	8.8-26.4	8.3-43.0	4.1-34.2	11.6-36.5	9.8-36.4

Table S2: Statistics related to the persistence of WRs in DJFM (fig. 12).

Persistence [days]	**NAO+**		**SBL**		**NAO-**		**AR**	
	Experiment		*Experiment*		*Experiment*		*Experiment*	
	control	hosing	control	hosing	control	hosing	control	hosing
Mean	5.0	6.8	4.8	4.1	6.6	5.2	4.4	4.3
Median	3	5	4	3	5	3	3	3
25^{th}-75^{th} percentile range	2-6	2-9	2-6	2-5	2-9	2-7	1-6	2-6
10^{th}-90^{th} percentile range	1-11	1-15	1-9	1-8	1-15	1-12	1-9	1-9